NANO LETTERS

Letter

Thermophoretic Motion of Water Nanodroplets Confined inside Carbon Nanotubes

Harvey A. Zambrano, Jens H. Walther, Petros Koumoutsakos, and Ivo F. Sbalzarini

Nano Lett., **2009**, 9 (1), 66-71 • DOI: 10.1021/nl802429s • Publication Date (Web): 23 December 2008

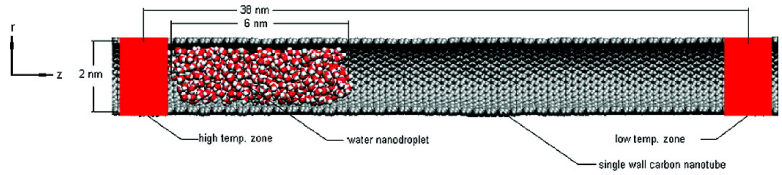

More About This Article

Additional resources and features associated with this article are available within the HTML version:

- Supporting Information
- Access to high resolution figures
- Links to articles and content related to this article
- Copyright permission to reproduce figures and/or text from this article

View the Full Text HTML

NANO LETTERS

2009
Vol. 9, No. 1
66-71

Thermophoretic Motion of Water Nanodroplets Confined inside Carbon Nanotubes

Harvey A. Zambrano,[†] Jens H. Walther,[*,†,‡] Petros Koumoutsakos,[‡] and Ivo F. Sbalzarini[§]

Department of Mechanical Engineering, Fluid Mechanics, Technical University of Denmark, DK-2800 Lyngby, Denmark, Computational Science and Engineering Laboratory, ETH Zurich, CH-8092, Switzerland, and Institute of Computational Science and Swiss Institute of Bioinformatics, ETH Zurich, CH-8092, Switzerland

Received August 9, 2008; Revised Manuscript Received December 5, 2008

ABSTRACT

We study the thermophoretic motion of water nanodroplets confined inside carbon nanotubes using molecular dynamics simulations. We find that the nanodroplets move in the direction opposite the imposed thermal gradient with a terminal velocity that is linearly proportional to the gradient. The translational motion is associated with a solid body rotation of the water nanodroplet coinciding with the helical symmetry of the carbon nanotube. The thermal diffusion displays a weak dependence on the wetting of the water−carbon nanotube interface. We introduce the use of the moment scaling spectrum (MSS) in order to determine the characteristics of the motion of the nanoparticles inside the carbon nanotube. The MSS indicates that affinity of the nanodroplet with the walls of the carbon nanotubes is important for the isothermal diffusion and hence for the Soret coefficient of the system.

Introduction. Open-ended nanotubes offer unique possibilities as fluid conduits with applications ranging from molecule separation devices in biocatalysis[1,2] to encapsulation media for drug storage and delivery.[1,3] Liquids and solids in nanochannels may be driven by electrophoresis, osmosis, gradients in the surface tension (Marangoni effect[4]), pressure gradients, and thermophoresis. Hence, electrophoresis has been used for driving electrically charged particles in nanosystems[5,6] and gradients in the surface tension have been exploited[7] to drive flow through carbon nanotubes (CNTs) immersed into a lipid membrane.[8] Pressure gradients imposed in nanopipes have been used to generate controlled flows for nanoscale applications[9] and to enhance electrophoretic motion across carbon nanotube membranes.[10] The use of thermal gradients to induce mass transport is known as thermophoresis, the Soret effect, or thermodiffusion.[11,12]

The first observation of thermodiffusion was reported by Ludwig[13] in 1856, who found differences in samples taken from different parts of a solution in which the temperature was not uniform. A systematic investigation of the phenomena was subsequently conducted by Soret[14] in 1879−1881 and by Ibbs[15,16] in 1921−1925 for thermodiffusion in gases. Ibbs found that the coefficient of thermal diffusion is more sensitive than any of the other transport coefficients to the nature of the intermolecular forces.[15,16] Thus, a complete understanding of the thermal diffusion could provide a powerful means of investigation of forces between molecules.[17] Although the theoretical explanation of thermodiffusion for molecules in liquids is still under debate,[18,19] the investigation of its practical usability is motivated by potential applications in nanotechnology. Hence, thermodiffusion was recently used as the driving mechanism in artificially fabricated nanomotors,[20] and thermodiffusion is expected to allow microscale manipulation and control of flow in nanofluidic devices.[20] In a recent theoretical study, thermophoresis was shown to induce motion of solid gold nanoparticles confined inside carbon nanotubes.[21] In the present investigation, we study thermophoretic motion of liquid water nanodroplets confined inside carbon nanotubes.

Numerical Methods. We perform molecular dynamics (MD) simulations using the MD package FASTTUBE.[22] The package has been used extensively to study water confined inside[23−26] and surrounding[27,28] carbon nanotubes. The potentials governing the water−carbon interaction have been calibrated against experiments by considering the contact angle of a water droplet on a graphite surface.[29−31] In the present MD simulations we use the rigid SPC/E water model[32] and describe the valence forces within the carbon

* Corresponding authors, jhw@mek.dtu.dk and walther@inf.ethz.ch.
† Department of Mechanical Engineering. Fluid Mechanics, DTU.
‡ Computational Science and Engineering Laboratory, ETH Zurich.
§ Institute of Computational Science and Swiss nstitute of Bioinformatics, ETH Zurich.

10.1021/nl802429s CCC: $40.75
Published on Web 12/23/2008

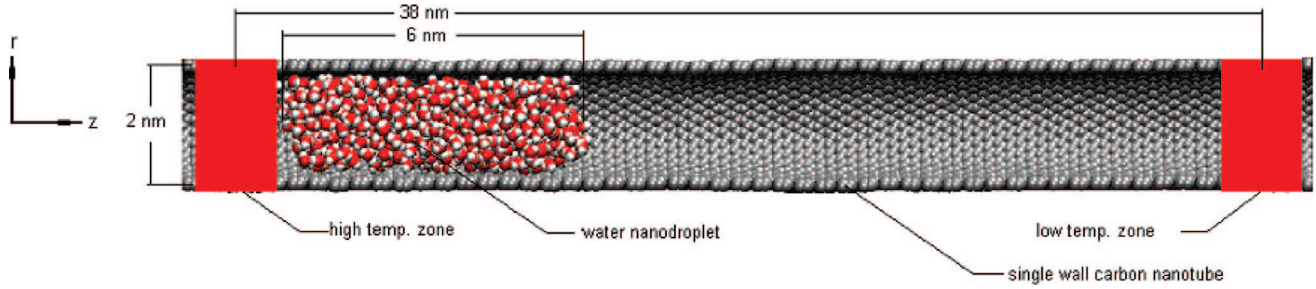

Figure 1. Schematic of the water nanodroplet confined inside a carbon nanotube. A thermal gradient is imposed by heating the end sections (in red) of the carbon nanotube.

Table 1. Parameters for the Carbon Interactions: K_r, r_c, and γ Are the Parameters of the Morse Potential, K_θ and θ_C Are the Angle Parameters, K_ϕ Is the Torsion Parameter, and ε_{CC} and σ_{CC} Are the Lennard-Jones Parameters of the Carbon−Carbon Interaction[a]

$K_r = 478.90$ kJ/mol	$r_c = 0.1418$ nm
$K_\theta = 562.2$ kJ/mol	$\theta_c = 120.00°$
$K_\phi = 25.12$ kJ/mol	$\gamma = 21.867$ nm^{-1}
$\varepsilon_{CC} = 0.4396$ kJ/mol	$\sigma_{CC} = 0.3851$ nm

[a] The incorrect units of K_r reported in ref 22 have been corrected.

nanotubes using Morse, harmonic angle, and torsion potentials,[22] thus

$$U(r_{ij}, \theta_{ijk}, \phi_{ijkl}) = K_r(\xi_{ij} - 1)^2 + \frac{1}{2}K_\theta(\cos\theta_{ijk} - \cos\theta_c)^2 + \frac{1}{2}K_\varphi(1 - \cos 2\phi_{ijkl}) \quad (1)$$

$$\xi_{ij} = e^{-r(r_{ij} - r_c)}$$

where r_{ij} denotes the bond length between two carbon atoms and θ_{ijk} and ϕ_{ijkl} are the bending and torsional angles. We include a nonbonded carbon−carbon Lennard-Jones potential to describe the van der Waals interaction between the carbon atoms in double-walled nanotubes

$$U_{LJ}(r_{ij}) = 4\varepsilon_{\alpha\beta}\left[\left(\frac{\sigma_{\alpha\beta}}{r_{ij}}\right)^{12} - \left(\frac{\sigma_{\alpha\beta}}{r_{ij}}\right)^{6}\right] \quad (2)$$

where $\varepsilon_{\alpha\beta}$ and $\sigma_{\alpha\beta}$ are the parameters of the potential, here $\varepsilon_{CC} = 0.4396$ kJ/mol and $\sigma_{CC} = 0.3851$ nm. Standard 1−2 and 1−3 nearest neighbor exclusion rules are applied. This additional Lennard-Jones term is excluded for the simulations of single-walled carbon nanotubes unless otherwise specified. The parameters of the carbon nanotube potentials are listed in Table 1.

The water−carbon interaction is modeled by a single Lennard-Jones term acting between the carbon and the oxygen of the water, consistent with the SPC/E water model. For the parameters of the potential, we use a constant σ_{CO} value of 0.3190 nm throughout the simulations but vary the ε_{CO} parameter in order to investigate the effect of wetting on the thermophoretic motion of the water nanodroplet. As a reference value we use $\varepsilon_{CO} = 0.3920$ kJ/mol, which was found to reproduce the experimental contact angle of 95.3° of a macroscopic water droplet on a graphite surface.[23,29] We furthermore use values of 0.2508 and 0.5643 kJ/mol corresponding to macroscopic contact angles of 127.8° and 50.7°, respectively.[23,29]

The nonbonded interactions, including van der Waals and Coulomb, are truncated at 1.0 nm. The Coulomb potential

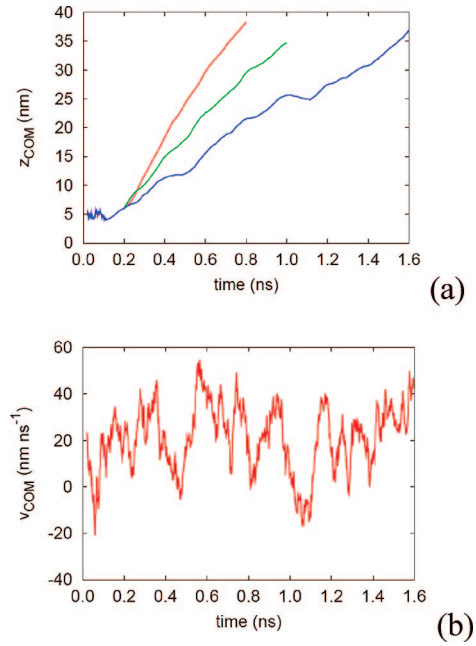

Figure 2. (a) Position of the center of mass of the nanodroplet (z_{COM}) as a function of the time for three different thermal gradients (red, 1.97 K/nm; green, 1.58 K/nm and blue, 1.05 K/nm). (b) Mean velocity of the center of mass of the nanodroplet (v_{COM}) as a function of the time for the case with thermal gradient of 1.05 K/nm.

is smoothed[22,33] to ensure conservation of energy. For a more detailed description of the potential models and parameters used in this investigation, we refer to refs 29 and 22 and reference therein.

The equations of motion are integrated in time using the leapfrog scheme with a time step of 2 fs. Periodic boundary conditions are imposed in the direction parallel to the tube axis and free space conditions in the normal directions. We equilibrate the system for 0.1 ns. During the equilibration we couple the water and the CNT to two separate Berendsen thermostats[34] with a time constant of 0.1 ps. After equilibration we impose a thermal gradient along the axis of the CNT. The heated zones are two 2 nm sections at the ends of the computational box as illustrated in Figure 1.

We study the effects of thermal gradients (∇T) ranging from 0.40 to 3.68 K/nm. We note that the lower gradients ($\nabla T < 1.0$ K/nm) are attainable experimentally[20] whereas the larger gradients help us assess trends and to increase the signal-to-noise ratio in our simulations.

We measure the position of the center of mass of the water nanodroplets (z_{COM}) and the corresponding center of mass

velocity (v_{COM}) during the simulation. Moreover, we measure the radial profiles of the density and the axial and tangential velocity of the water nanodroplet. The profiles are sampled in the central region of the droplet and exclude the free surface at the droplet caps. The resolution of the binning is 0.117 nm for the radial profiles. The coefficient of thermal diffusion (D_t) is estimated from

$$D_t = \frac{v_{COM}}{\nabla T} \tag{3}$$

The Soret coefficient is defined as[11,12,18,35]

$$S_t = \frac{D_t}{D} \tag{4}$$

where D is the isothermal diffusion coefficient. We determine D from the moment scaling spectra (MSS)[36−38] with a temporal resolution of 2 ps. Each trajectory is represented as a sequence $z_{COM}(n)$ of the $n = 1,...,M$ position of the center of mass over time. The time difference between two points is given by $\delta t = \Delta n*2$ ps. Our analysis is based on computing the first 6 moments of displacement

$$\mu_\nu(\Delta n) = \frac{1}{M-\Delta n}\sum_{n=1}^{M-\Delta n} |z_{COM}(n+\Delta n) - z_{COM}(n)|^\nu \tag{5}$$

for $\nu = 0,..., 6$ and $\Delta n = 1,..., M/3$. This includes the classical mean square displacement (MSD) as the special case where $\nu = 2$. We assume each moment μ to depend on the time shift $\delta t = \Delta n*2$ ps in a power law[36]

$$\mu_\nu(\delta t) = 2dD_\nu(\delta t)^{\gamma_\nu} \tag{6}$$

where $d = 1$ is the dimension of the space. The scaling coefficients γ_ν are thus determined by linear least-squares regression of $\log(\mu_\nu)$ vs $\log(\delta t)$. For $\nu = 2$ we obtain the isothermal diffusion coefficient $D = D_2$ from the y axis intercept y_0 as $D = 0.5 \times 10^{y0}$. The plot of γ_ν vs ν is called the moment scaling spectrum (MSS);[36] for all strongly self-similar diffusion processes, the MSS shows a straight line through the origin. The slope S_{MSS} of this line is determined using linear least-squares regression. $S_{MSS} = 0.5$ indicates pure normal diffusion, $S_{MSS} = 1.0$ is characteristic for ballistic motion. Superdiffusive processes have $0.5 < S_{MSS} < 1.0$, and subdiffusion $0.0 < S_{MSS} < 0.5$. MSS analysis is robust against noise in the trajectory and allows more accurate regression due to the almost perfect linearity of the MSS and the fact that S_{MSS} has a smaller estimator variance than γ_2. In addition it enables classification of different motion types with uniform sensitivity along the trajectory.

Results. In this investigation we perform molecular dynamics simulations of a water nanodroplet confined inside a carbon nanotube (Figure 1) subject to a thermal gradient. We use a zigzag carbon nanotube with a chiral vector of (30,0) which corresponds to a radius of 1.17 nm and a pitch angle of helical symmetry (α_{zz}) of ±60°.[39,40] The size of the computational domain along the axis of the carbon nanotube is 42.6 nm which requires 12000 carbon atoms. The water droplet consists of 514 water molecules and the confinement results in a droplet mean radius of approximately 0.95 nm and length 6.00 nm; cf. Figure 1.

We impose thermal gradients of 0.00, 0.40, 0.52, 0.79, 1.05, 1.32, 1.58, 1.71, 1.97, 2.10, 2.63, 2.89, 3.16, and 3.68 K/nm. We observe, for the nonzero gradients, a thermophoretic motion of the water nanodroplets in the direction opposite the thermal gradient (Figure 2a). Moreover, the center of mass velocity of the water nanodroplet increases as higher gradients are imposed. The mean terminal velocity of the nanodroplet is approximately 22 m/s for a thermal gradient of 1.05 K/nm, cf. Figure 2b, and similar in magnitude to the terminal velocity of 25 m/s found in the

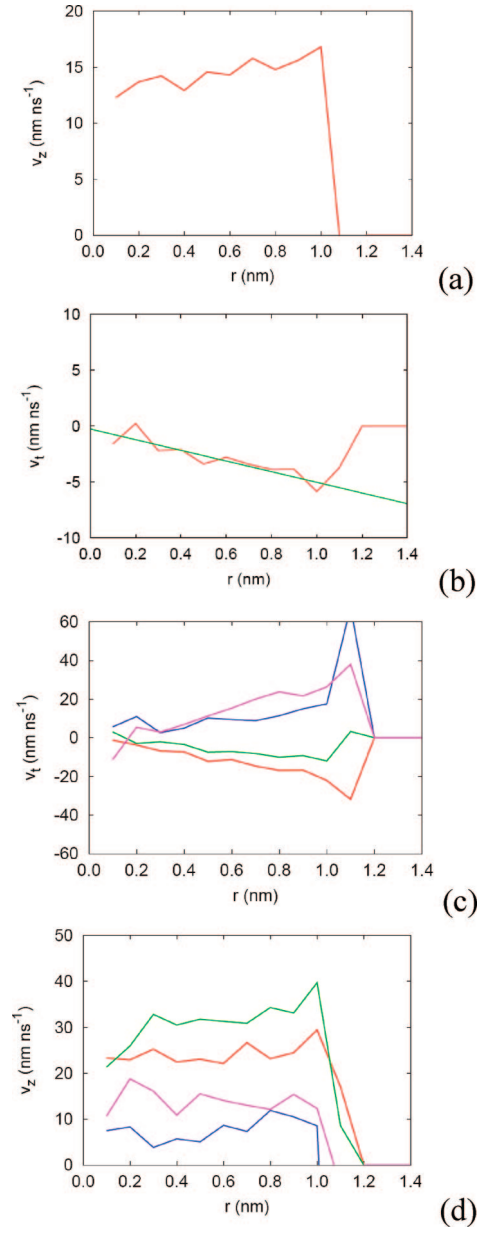

Figure 3. The radial profiles of the axial and tangential velocity of a water nanodroplet confined inside single-walled carbon nanotubes subject to a thermal gradient of 1.05 K/nm. (a) Time average axial velocity profile (v_z). (b) Time average tangential velocity (v_t): the red line represents the measured velocity profile and the green line the best fit to a solid body rotation. (c) Tangential velocity profiles for different time intervals (red line, 0.56−0.70 ns; green line, 0.70−0.92 ns; blue line, 0.92−1.04 ns; pink line, 1.04−1.20 ns). (d) Axial velocity profiles for different time intervals (red line, 0.56−0.70 ns; green line, 0.70−0.92 ns; blue line, 0.92−1.04 ns; pink line, 1.04−1.20 ns).

previous study of thermophoretic motion of gold nanoparticles confined inside carbon nanotubes.[39]

The axial velocity profile (v_z) of the water nanodroplets displays a maximum value in the vicinity of the fluid−solid interface (Figure 3a). Hence the fluid motion of the water nanodroplets exhibits recirculation in a frame of reference fixed to the center of mass of the nanodroplet. The corresponding tangential velocity profile (v_t) shown in Figure 3b displays a solid body rotation similar to the rotation of the solid gold nanoparticle observed in our previous study.[39]

The motion is associated with large temporal fluctuations, cf. Figure 2b and Figure 3c, which are related to the change in the direction of rotation; cf. Figure 3c. Moreover, the angle of rotation appears to be correlated to the two possible paths imposed by the chirality vector of the carbon nanotubes of ±60°.[39] From the simulations (Figure 3c,d) we find an angle between the maximum value of the tangential velocity, measured in the vicinity of the surface of the carbon nanotube, and the axial velocity of the nanodroplet, has a mean value of approximately ±67°. Thus, the rotation of the nanodroplet is determined by the helical symmetry of the CNT.

In order to determine the isothermal diffusion coefficient, we carry out long (200 ns) simulations of the water nanodroplet confined inside the carbon nanotube with zero temperature gradient. Below time scales of about 200 ps, the scaling of the moments of displacement indicates ballistic motion (see Figure 4a) with $S_{MSS} = 0.97$. The scaling plot then shows a pronounced kink, with a long time scaling that is characteristic for diffusive motion (see MSS plot in Figure 4b). In this diffusive regime we find an isothermal diffusion coefficient of 8.8 nm^2/ns with $S_{MSS} = 0.46$, indicating pure normal diffusion. This value is in reasonable agreement with values previous obtained for water under nanoscale confinement ($D = 0.94-5.7$ nm^2/ns).[41−43]

For the simulations with a nonzero thermal gradient, we observe a linear increase in the center of mass velocity as function of the thermal gradient (Figure 5a) which confirms that the motion is thermophoretic. We expect that the motion is related to high-frequency phonon vibrations of the carbon nanotubes, i.e., the kinetic pressure of the carbon nanotubes as demonstrated in ref 21. We note that the present classical formulation will excite all phonons simultaneously, whereas a full quantum description will suppress high-frequency phonons at low temperatures. Thus, the speed of the nanodroplets may be quantized at low temperatures.

The extracted coefficient of thermal diffusion is 20.9 nm^2/(ns K), which corresponds to a Soret coefficient of 2.37 K^{-1}. This value is 3 orders of magnitude larger than the coefficients reported by Platten et al.[12] and Saghir et al.[44] for mixtures of water−methanol and by Reith and Muller-Plathe[45] of binary Lennard-Jones liquids.

In order to evaluate the influence of the wetting of the water−carbon interface on the thermophoretic motion of the nanodroplet, we vary the Lennard-Jones parameter ε_{co}, from the reference value of 0.3920 kJ/mol to 0.5643 and 0.2508 kJ/mol, which correspond to strongly hydrophilic and strongly hydrophobic interfaces, respectively. The resulting

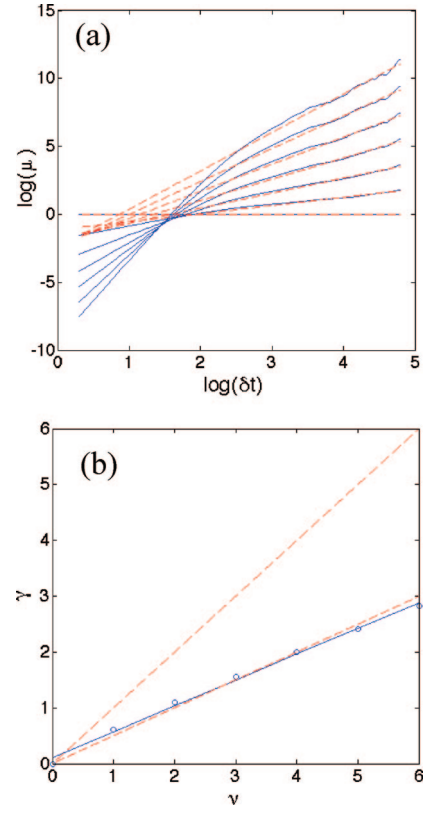

Figure 4. (a) Moments of displacement for the simulations using $\varepsilon_{co} = 0.3920$ kJ/mol. Solid blue lines show the temporal scaling of the first six moments of displacement. The least-squares fits are indicated by red dashed lines. The scaling coefficients are given by the slopes of the dashed lines. On time scales below 200 ps, the scaling corresponds to ballistic motion. Diffusive behavior with $D = 8.8$ nm^2/ns is recovered for longer time scales. (b) Moment scaling spectrum. The circles mark the scaling coefficients as computed from the fits in (a); the solid blue line indicates the linear least-squares fit with a slope of $S_{MSS} = 0.46$. The red dashed lines of slopes 0.5 and 1.0 show the theoretically expected spectra for pure normal diffusion and ballistic motion, respectively.

water density profiles display the characteristic structure at the interface with enhanced structure for increasing hydrophobicity (Figure 5b).

We observe a small but systematic change in the center of mass velocity of the water nanodroplet, cf. Figure 5a, and the coefficients of thermal diffusion vary from the reference value of 20.9 nm^2/(ns K) to 18.8 nm^2/(ns K) for the strongly hydrophilic interface to 23.1 nm^2/(ns K) for the strongly hydrophobic interface. This behavior is consistent with the increased surface adhesion and reduced isothermal diffusion for the hydrophilic interface. Conversely, the superhydrophobic interface exhibits a reduced adhesion and hence increased isothermal diffusion as shown in Figure 5a.

To estimate the effect of wetting on the Soret coefficient, we repeat the long (200 ns) isothermal simulations for the system setting with different ε_{co} values. From these simulations we measure an isothermal diffusion coefficient of 20.8 nm^2/ns ($S_{MSS} = 0.46$) and 7.9 nm^2/ns ($S_{MSS} = 0.54$) for ε_{co} values of 0.2508 and 0.5643 kJ/mol, respectively. The corresponding Soret coefficients are $S_t = 0.90$ K^{-1} and $S_t = 2.92$ K^{-1}. Hence, the hydrophilic interface exhibits a higher

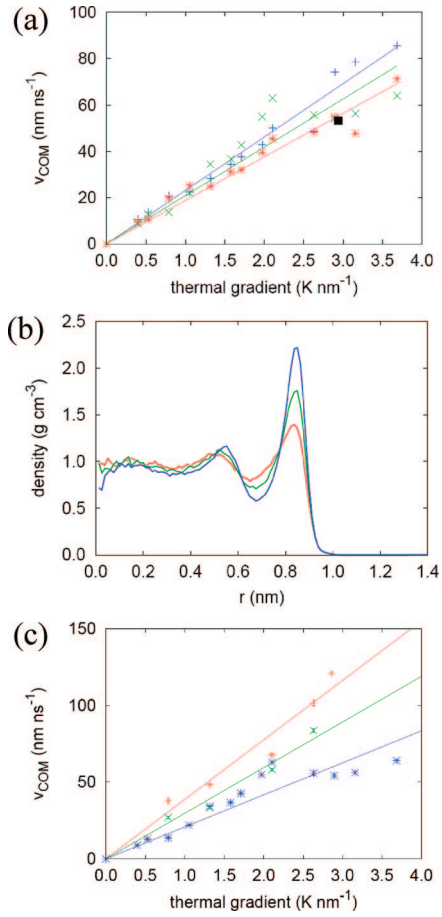

Figure 5. Influence of wetting effect and chirality on the center of mass mean velocity and on the density profile of a water nanodroplet confided inside a zigzag carbon nanotube. (a) Mean velocity of the center of mass v_{com} as a function of the imposed thermal gradient for three different ε_{co} values (red line, $\varepsilon_{co} = 0.5643$ kJ/mol; green line, $\varepsilon_{co} = 0.3920$ kJ/mol; and blue line, $\varepsilon_{co} = 0.2508$ kJ/mol). Red (∗), green (×), and blue (+) represent the particular mean velocities of each case simulated. A black square represents the mean velocity of the center of mass of a nanodroplet confined inside a double-walled carbon nanotube with an imposed thermal gradient of 2.83 K/nm. (b) Radial density profile for the three different ε_{co} values (red line, $\varepsilon_{co} = 0.2508$ kJ/mol; green line, $\varepsilon_{co} = 0.3920$ kJ/mol; blue line, $\varepsilon_{co} = 0.5643$ kJ/mol). (c) Influence of chirality on the center of mass mean velocity of a water nanodroplet confined inside a carbon nanotube. Chirality: Red (+) (17,17), green (×) (20,14), and blue (∗) (30,0).

Soret coefficient than the hydrophobic interfaces, mainly caused by large change in the isothermal diffusion.

We finally consider the thermophoretic motion of a water nanodroplet confined inside single carbon nanotubes of different chirality and inside double-walled carbon nanotubes. The additional single-walled carbon nanotubes include (17,17) armchair and (24,14) chiral carbon nanotubes, both with a diameter similar to the zigzag (30,0) carbon nanotubes previously considered. For all the different chiralities we observe a consistent thermophoretic motion of the water nanodroplets as shown in Figure 5c. Moreover, we find that the nanodroplet moves with the highest velocity inside the (17,17) armchair carbon nanotubes and with the lowest velocity inside the zigzag (30,0) carbon nanotubes. These results are in agreement with recent molecular dynamics and quantum chemistry studies of self-diffusion of water confined inside armchair and zigzag carbon nanotubes.[46]

For the double walled carbon nanotubes, we impose a thermal gradient of 2.83 K/nm and observe a thermophoretic motion (solid black square in Figure 5a) similar to that observed for single-walled carbon nanotubes. The terminal center of mass velocity is 53 m/s and similar to the velocity observed for the hydrophilic ($\varepsilon_{co} = 0.5643$ kJ/mol) single-walled carbon nanotube of 55 m/s. This behavior is consistent with the enhanced water−carbon interaction due to the presence of the second layer of carbon atoms.

Conclusions. The present molecular dynamics simulations have demonstrated that water nanodroplets may be driven through single- and double-walled carbon nanotubes by imposing a thermal gradient along the axis of the carbon nanotube. The driving force is thermophoretic, and the resulting thermal diffusion involves both a translational and rotational motion of the nanodroplets. The rotation is imposed by the helical symmetry of the carbon nanotubes. We find a weak influence of wetting on thermophoresis, but a strong influence on the isothermal diffusion and hence the Soret coefficient. In summary, thermophoresis may be a viable mechanism for controlling the motion of water nanodroplets confined inside a single- and double-walled carbon nanotubes.

Acknowledgment. This research has been supported in part by the Danish Research Council (Grant No. 274-06-0465), the Danish Center for Scientific Computing (DCSC), and the Myhrwold and Otto Mønsted Foundations. The authors wish to acknowledge discussion with Richard Jaffe, Dimos Poulikakos, and Efthimios Kaxiras.

References

(1) Kalra, A.; Garde, S.; Hummer, G. *Proc. Natl. Acad. Sci. U.S.A.* **2003**, *100*, 10175–10180.
(2) Mitchell, D. T.; Lee, S. B.; Trofin, L.; Li, N.; Nevanen, T. K.; Soderlund, H.; Martin, C. R. *J. Am. Chem. Soc.* **2002**, *124*, 11864–11865.
(3) Gasparac, R.; Kohli, P.; Mota, M. O.; Trofin, L.; Martin, C. R. *Nano Lett.* **2004**, *4*, 513–516.
(4) Marangoni, C. *Ann. Phys. Chem.* **1871**, *143*, 337.
(5) Gogotsi, Y.; Libera, J. A.; Güvenc-Yazicioglu, A.; Megaridis, C. M. *Appl. Phys. Lett.* **2001**, *79*, 1021–1023.
(6) Tokarz, M.; Akerman, B.; Olofsson, J.; Joanny, J. F.; Dommersnes, P.; Orwar, O. *Proc. Natl. Acad. Sci. U.S.A.* **2005**, *102*, 9127–9132.
(7) Zhou, J. J.; Noca, F.; Gharib, M. *Nanotechnology* **2006**, 4845–4853.
(8) Dommersnes, P. G.; Orwar, O.; Brochard-Wyart, F.; Joanny, J. F. *Europhys. Lett.* **2005**, *70* (2), 271–227.
(9) Holt, J. K.; Park, H. G.; Wang, Y.; Stadermann, M.; Artyukhin, A. B.; Grigoropoulos, C. P.; Noy, A.; Bakajin, O. *Science* **2006**, *312*, 1034.
(10) Vo-Dinh, T.; Cullum, B. M.; Stokes, D. L. *Sens. Actuators, B* **2001**, *74*, 2–11.
(11) Duhr, S.; Braun, D. *Proc. Natl. Acad. Sci. U.S.A.* **2006**, *103*, 19678–19682.
(12) Dutrieux, J. F.; Platten, J. K.; Chavepeyer, G.; Bou-Ali, M. M. *J. Phys. Chem. B* **2002**, *106*, 6104–6114.
(13) Ludwig, C. *S. Bayer Akad. Wiss. (Vienna)* **1856**, *20*, 539.
(14) Soret, C. *Ann. Chim. (Phys.)* **1881**, *22* (5), 293.
(15) Ibbs, T. L. *Proc. R. Soc. London* **1921**, *A99*, 385.
(16) Ibbs, T. L. *Physica IV* **1937**, *10*, 1133–1140.
(17) Grez, K. E. In *Transport Phenomena in Fluids*; Hanley, H. J. M., Eds.; Marcel Dekker: New York, 1969; Vol. 10, pp 333−376.
(18) Brenner, H. *Phys. Rev. E.* **2006**, *74* (1−20), 036306.
(19) Regazzetti, A.; Hoyos, M.; Martin, M. *J. Phys. Chem. B* **2004**, *108*, 15285–15292.
(20) Barreiro, A.; Rurali, R.; Hernandez, E. R.; Moser, J.; Pichler, T.; Forro, L.; Bachtold, A. *Science* **2008**, *320*, 775–778.

(21) Schoen, P. A. E.; Walther, J. H.; Poulikakos, D.; Koumoutsakos, P. *Appl. Phys. Lett.* **2007**, *90* (1−3), 253116.
(22) Walther, J. H.; Jaffe, R.; Halicioglu, T.; Koumoutsakos, P. *J. Phys. Chem. B* **2001**, *105*, 9980–9987.
(23) Werder, T.; Walther, J. H.; Jaffe, R. L.; Halicioglu, T.; Noca, F.; Koumoutsakos, P. *Nano Lett.* **2001**, *1* (12), 697–702.
(24) Zimmerli, U.; Gonnet, P. G.; Walther, J. H.; Koumoutsakos, P. *Nano Lett.* **2005**, *5* (6), 1017–1022.
(25) Kotsalis, E. M.; Walther, J. H.; Koumoutsakos, P. *Int. J. Multiphase Flow* **2004**, *30*, 995–1010.
(26) Kassinos, S. C.; Walther, J. H.; Kotsalis, E. M.; Koumoutsakos, P. *Lect. Notes Comput. Sci. Eng.* **2004**, *39*, 215–226.
(27) Walther, J. H.; Jaffe, R. L.; Kotsalis, E. M.; Werder, T.; Halicioglu, T.; Koumoutsakos, P. *Carbon* **2004**, *42*, 1185–1194.
(28) Walther, J. H.; Werder, T.; Jaffe, R. L.; Koumoutsakos, P. *Phys. Rev. E.* **2004**, *69*, 062201.
(29) Werder, T.; Walther, J. H.; Jaffe, R. L.; Halicioglu, T.; Koumoutsakos, P. *J. Phys. Chem. B* **2003**, *107*, 1345–1352.
(30) Jaffe, R. L.; Gonnet, P.; Werder, T.; Walther, J. H.; Koumoutsakos, P. *Mol. Simul.* **2004**, *30* (4), 205–216.
(31) Walther, J. H.; Werder, T.; Jaffe, R. L.; Gonnet, P.; Bergdorf, M.; Zimmerli, U.; Koumoutsakos, P. *Phys. Chem. Chem. Phys.* **2004**, *6*, 1988–1995.
(32) Berendsen, H. J. C.; Grigera, J. R.; Straatsma, T. P. *J. Phys. Chem.* **1987**, *91*, 6269–6271.
(33) Levitt, M.; Hirshberg, M.; Laidig, K. E.; Daggett, V. *J. Phys. Chem. B* **1997**, *101*, 5051–5061.
(34) Berendsen, H. J. C.; Postma, J. P. M.; van Gunsteren, W. F.; DiNola, A.; Haak, J. R. *J. Chem. Phys.* **1984**, *81*, 3684–3690.
(35) Platten, J. K. *J. Appl. Mech.* **2006**, *73*, 5–15.
(36) Ferrari, R.; Manfroi, A. J.; Young, W. R. *Physica D* **2001**, *152*, 111–137.
(37) Ewers, H.; Smith, A. E.; Sbalzarini, I. F.; Lilie, H.; Koumoutsakos, P. *Proc. Natl. Acad. Sci. U.S.A.* **2005**, *102* (402), 15110–15115.
(38) Sbalzarini, I. F.; Koumoutsakos, P. *J. Struct. Biol* **2005**, *151* (2), 182–195.
(39) Schoen, P. A. E.; Walther, J. H.; Arcidiacono, S.; Poulikakos, D.; Koumoutsakos, P. *Nano Lett.* **2006**, *6*, 1910–1917.
(40) Belikov, A. V.; Lozokiv, Y. E.; Nikolaev, A. G.; Popov, A. M. *Chem. Phys. Lett.* **2004**, *385*, 72–78.
(41) Striolo, A. *Nano Lett.* **2006**, *6* (1), 633–639.
(42) Van Hijkoop, V. J.; Dammers, A. J.; Malek, K.; Coppens, M. O. *J. Chem. Phys.* **2007**, *127*, 085101.
(43) Sega, M.; Vallauri, R.; Melchionna, S. *Phys. Rev. E* **2005**, *72*, 041201.
(44) Saghir, M. Z.; Jiang, C. G.; Derawi, S. O.; Stenby, E. H.; Kawaji, M. *Eur. Phys. J. E* **2004**, *15*, 241–247.
(45) Reith, D.; Muller-Plathe, F. *J. Chem. Phys.* **2000**, *112* (5), 2436–2443.
(46) Liu, Y.-C.; Shen, J.-W.; Gubbins, K. E.; Moore, J. D.; Wu, T.; Wang, Q. *Phys. Rev. B* **2008**, *77*, 125438 .

NL802429S